Model. Earth Syst. Environ. (2016) 2:30
DOI 10.1007/s40808-016-0082-1

ORIGINAL ARTICLE

Interpretation of gravity and magnetic anomaly over thin sheet-type structure using very fast simulated annealing global optimization technique

Arkoprovo Biswas[1]

Received: 21 December 2015 / Accepted: 9 January 2016 / Published online: 4 February 2016

Abstract A Very Fast Simulated Annealing (VFSA) global optimization algorithm is developed for interpretation of gravity and magnetic anomaly over thin sheet type structure for ore exploration. The results of VFSA optimization show that it can uniquely determine all the model parameters without any uncertainty. Inversion of noise-free and noisy synthetic data for single structures as well as field data demonstrates the efficacy of the approach. The technique has been vigilantly and efficaciously applied to two real data examples from Canada with the presence of ore bodies. In both Model examples, the model parameters acquired by the present method, mostly the shape and depth of the buried structures were found to be in respectable agreement with the actual parameters. The present method has the proficiency of evading highly noisy data points and enhances the interpretation results. The technique can be extremely appropriate for mineral exploration, where the gravity and magnetic data is observed due to ore body of sheet like structure embedded in the shallow and deeper subsurface. The computation time for the whole process is very short.

Keywords Gravity and magnetic anomaly · Sheet type structure · VFSA · Ore exploration

✉ Arkoprovo Biswas
arkoprovo@gmail.com

[1] Department of Earth and Environmental Sciences, Indian Institute of Science Education and Research (IISER) Bhopal, Bhopal By-pass Road, Bhauri, Bhopal, Madhya Pradesh 462 066, India

Introduction

In most of the geophysical exploration problems, it is assumed that a geological structure that can be characterised passably by different sheet type structures. The model is frequently used in both gravity as well as magnetic interpretation to find the depth and other parameters of geological structures. Appraisal of the depth of a buried structure from the gravity and magnetic data has drawn considerable attention in exploration of minerals (Biswas et al. 2014a, b; Mandal et al. 2015, 2013). Wide interpretation procedures have been developed to interpret the gravity and magnetic data assuming fixed source geometrical models. In almost all the cases, these methods consider the diverse parameters of the buried body being a priori assumed, and the parameters may thereafter be obtained by different interpretation methods.

Many interpretation techniques were developed in the past and many new inversion methodologies are also present in the recent times. The techniques include graphical methods (Nettleton 1962, 1976), curves matching standardized techniques (Gay 1963, 1965; McGrath 1970), Fourier transform (Odegard and Berg 1965; Bhattacharyya 1965; Sharma and Geldart 1968), Euler deconvolution (Thompson 1982), Mellin transform (Mohan et al. 1986), Hilbert transforms (Mohan et al. 1982), Monograms (Prakasa Rao et al. 1986), least squares minimization approaches (Gupta, 1983; Silva 1989; McGrath and Hood 1973; Lines and Treitel 1984; Abdelrahman 1990; Abdelrahman et al. 1991; Abdelrahman and El-Araby 1993; Abdelrahman and Sharafeldin 1995a), ratio methods (Bowin et al. 1986; Abdelrahman et al.1989), characteristic points and distance approaches (Grant and West 1965; Abdelrahman 1994), neural network (Elawadi et al. 2001), Werner deconvolution (Hartmann et al. 1971; Jain 1976; Kilty 1983); Walsh

Transformation (Shaw and Agarwal 1990), Continual least-squares methods (Abdelrahman and Sharafeldin 1995b; Abdelrahman et al. 2001a, b; Essa 2012, 2013), Euler deconvolution method (Salem and Ravat 2003), Fair function minimization procedure (Tlas and Asfahani 2011a; Asfahani and Tlas 2012), DEXP method (Fedi 2007), deconvolution technique (Tlas and Asfahani 2011b); Regularised inversion (Mehanee 2014); Simplex algorithm (Tlas and Asfahani 2015). Recently simulated annealing methods (Gokturkler and Balkaya 2012), Very fast simulated annealing (Biswas 2015; Biswas and Sharma 2015; 2014a, b; Sharma and Biswas 2013) and particle swarm optimization (Singh and Biswas 2016) have been used to solve similar kind of non-linear inversion problems for different type of subsurface structures. Many other interpretation methods for gravity and magnetic data can be found in various literatures (Abdelrahman and Essa 2015, Abdelrahman and Sharafeldin 1996; Abdelrahman 1994; Asfahani and Tlas 2007, 2004; Tlas et al. 2005).

In the present work, Very fast simulated annealing (VFSA) is used to determine the various model parameters related to thin sheet type structures for gravity and magnetic anomalies. Since, VFSA optimization is able to search a enormous model space without negotiating the resolution and has the ability to avoid becoming trapped in local minima (Sen and Stoffa 2013; Sharma and Kaikkonen 1998, 1999a, b; Sharma and Biswas 2011, 2013 Sharma 2012; Biswas and Sharma 2015, 2016) and is used in interpreting the gravity and magnetic anomaly data. The applicability of the proposed technique is appraised and discussed with the help of synthetic data and two field examples. The method can be used to interpret the gravity and magnetic anomalies occurred due to a thin sheet type mineralized bodies.

Theory

Forward modeling

The general expression of a gravity anomaly *g(x)* for thin sheet at any point on the surface (Fig. 1) is given by the equations (after Gay 1963):

$$g(x) = k\left[\frac{x_0 \sin\theta + z\cos\theta}{x_0^2 + z^2}\right] \quad (1)$$

The general expression of a magnetic anomaly *m(x)* for thin sheet at any point on the surface (Fig. 1) is given by the equations (after Siva Kumar Sinha and Ram Babu 1985):

$$m(x) = k\left[\frac{x_0 \cos\theta + z\sin\theta}{x_0^2 + z^2}\right] \quad (2)$$

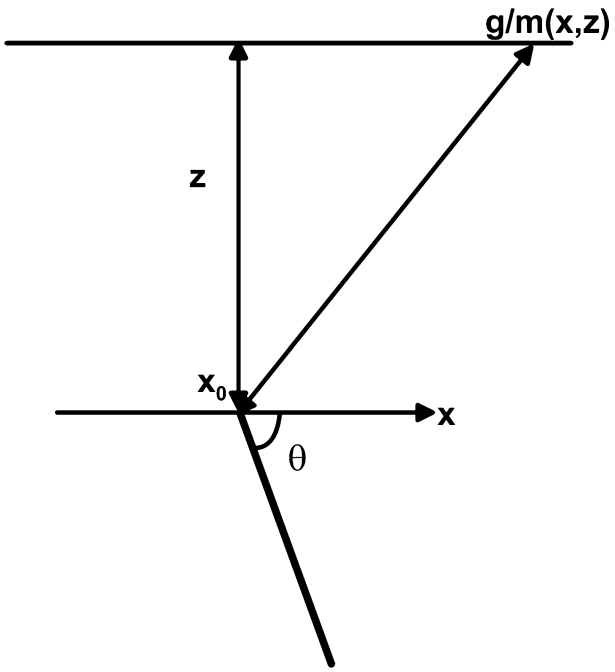

Fig. 1 A diagram showing cross-sectional views, geometries and parameters for thin sheet type structure

where, k is the amplitude coefficient, z is the depth from the surface to the top of the body (Thin Sheet), x_0 (i = 1,…,N) is the horizontal position coordinate, θ is the angle.

Inversion: Very Fast simulated annealing global optimization

The Global optimization methods such as simulated annealing, genetic algorithms, artificial neural networks and particle swarm optimization have been used in various geophysical data sets (e.g., Rothman 1985, 1986; Dosso and Oldenburg 1991; Sen and Stoffa 2013; Sharma and Kaikkonen 1998, 1999a, b; Zhao et al. 1996; Juan et al. 2010; Sharma and Biswas 2011, 2013; Sharma 2012; Biswas and Sharma 2014a, b, 2015; Biswas 2015; Singh and Biswas 2016). The Very Fast Simulated Annealing (VFSA) is a global optimization method is used for finding the global minimum of a function. The process comprises of heating a solid in a heat bath and then slowly allowing them to cool down and anneal into a state of minimum energy. The same principal when used to geophysical inversion aims to minimize an objective function called error function. The error function is analogous to the energy function in a way that error function is directly proportional to the degree of misfit between the observed data and the computed data.

The following misfit (φ) between the observed and model response is used for data interpretation (Sharma and Biswas 2013).

Table 1 Actual model parameters, search range and interpreted mean model for noise free and 10 % Gaussian noise with uncertainty-Gravity data (Model 1)

Model parameters	Actual value	Search range	Mean model	
			Noise-free	Noisy
k (mGal)	500	0–1000	499.7 ± 1.0	486.5 ± 1.8
x_0 (m)	150	0–300	150.0 ± 0.0	150.8 ± 0.2
z (m)	20	0–50	20.0 ± 0.0	19.4 ± 0.1
θ (°)	60	0–90	60.0 ± 0.0	60.7 ± 0.2
Misfit			2.5×10^{-8}	1.0×10^{-3}

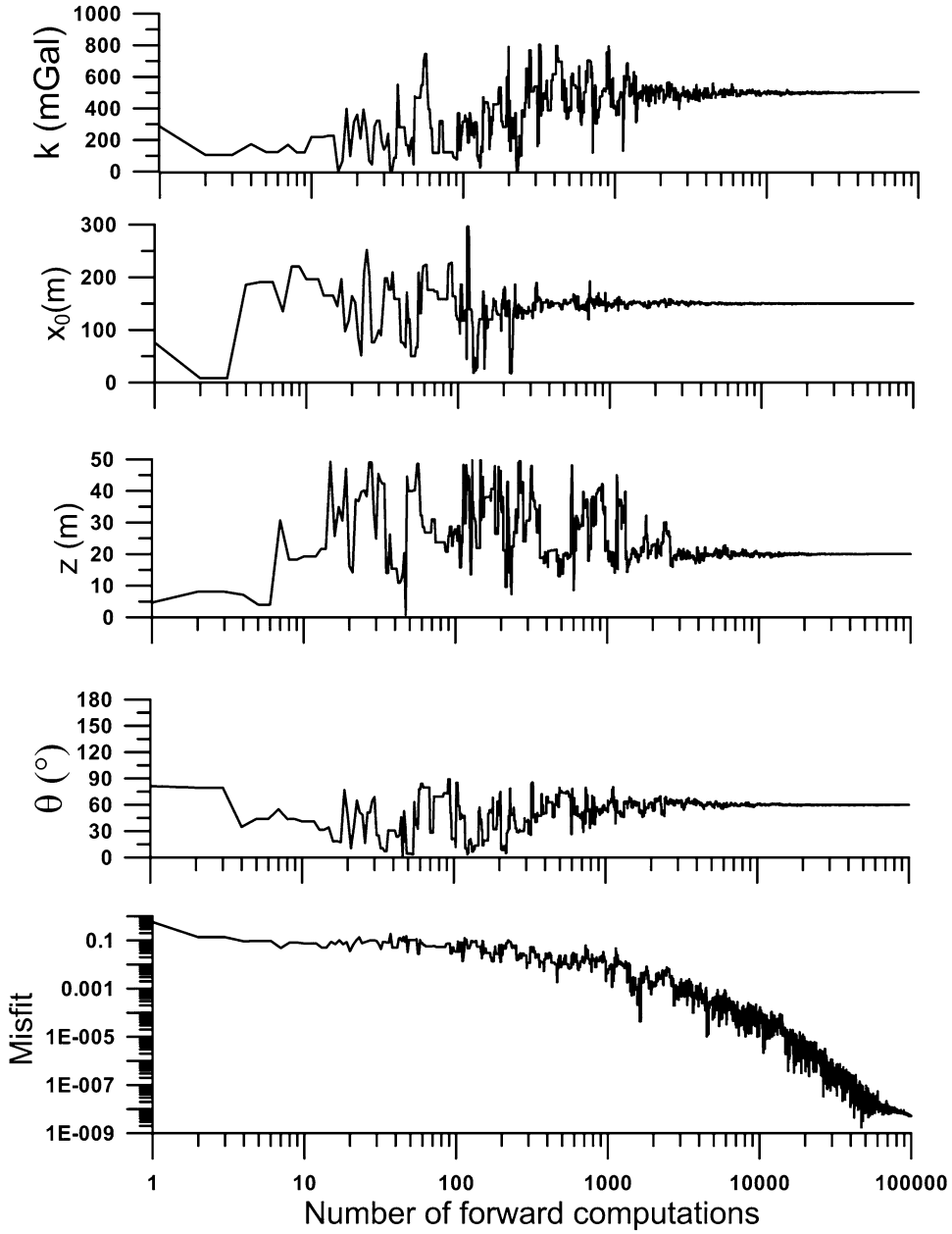

Fig. 2 Convergence pattern for various model parameters and misfit for gravity data

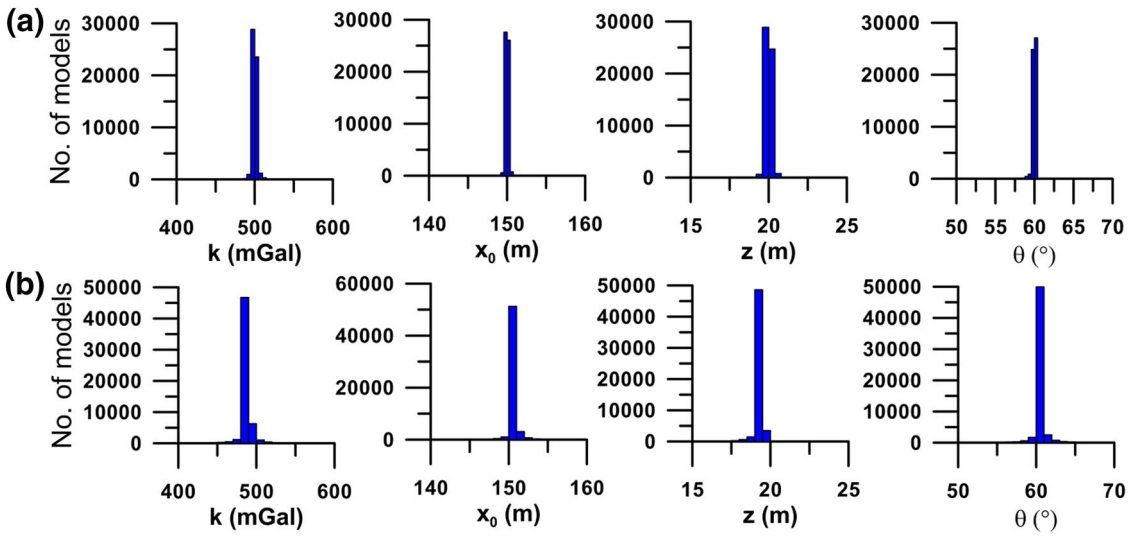

Fig. 3 Gravity data: **a** histograms of all accepted models having misfit $<10^{-4}$ for noise-free synthetic data for thin sheet-Model 1 and **b** histograms of all accepted models having misfit $<10^{-2}$ for noisy synthetic data for Thin sheet-Model 2

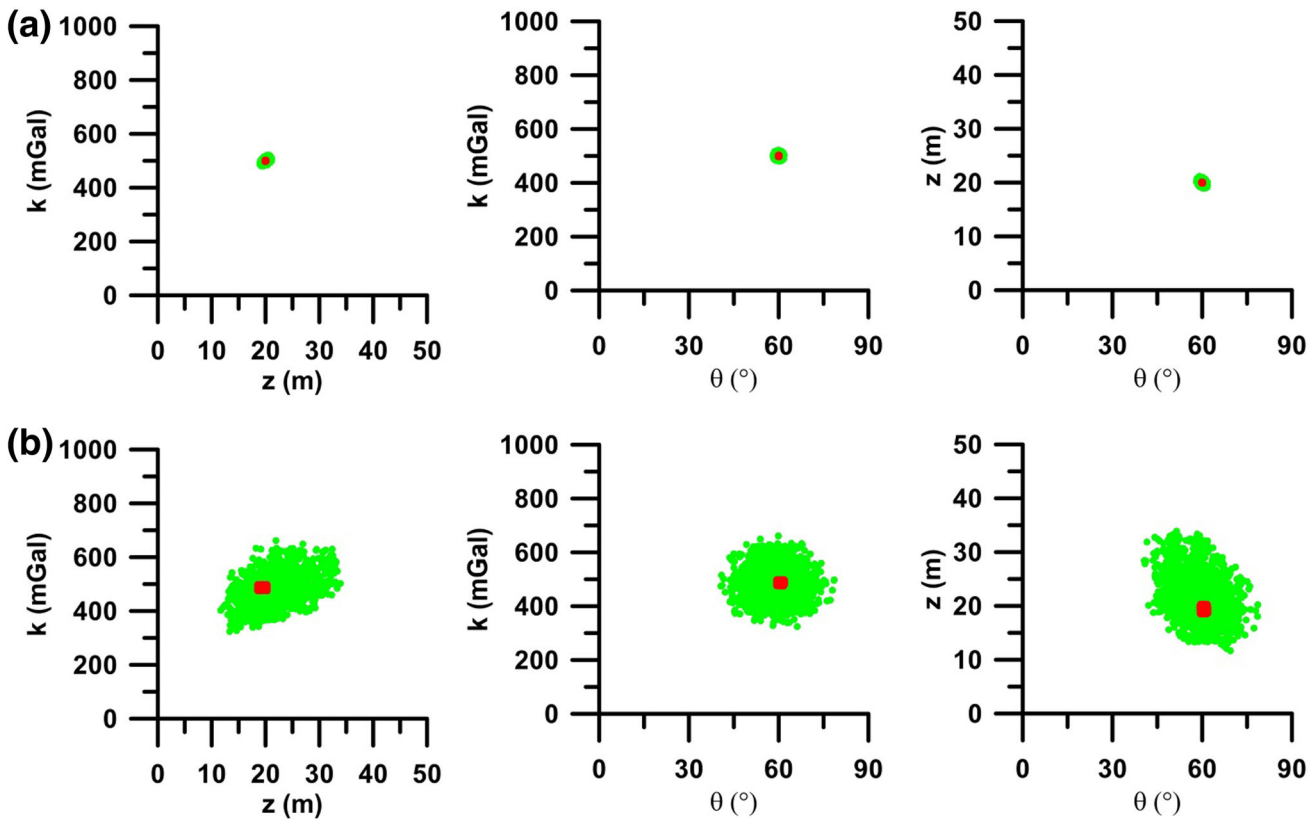

Fig. 4 Gravity data: **a** *scatter-plots* between amplitude coefficient (k), depth (z), magnetization angle (θ) for all models having misfit <threshold (10^{-4} for noise-free data) (*green*), and models with PDF >60.65 % (*red*) for noise free data; **b** scatter-plots between amplitude coefficient (k), depth (z), magnetization angle (θ) for all models having misfit <threshold (10^{-2} for noisy data) (*green*), and models with PDF >60.65 % (*red*) for noisy data

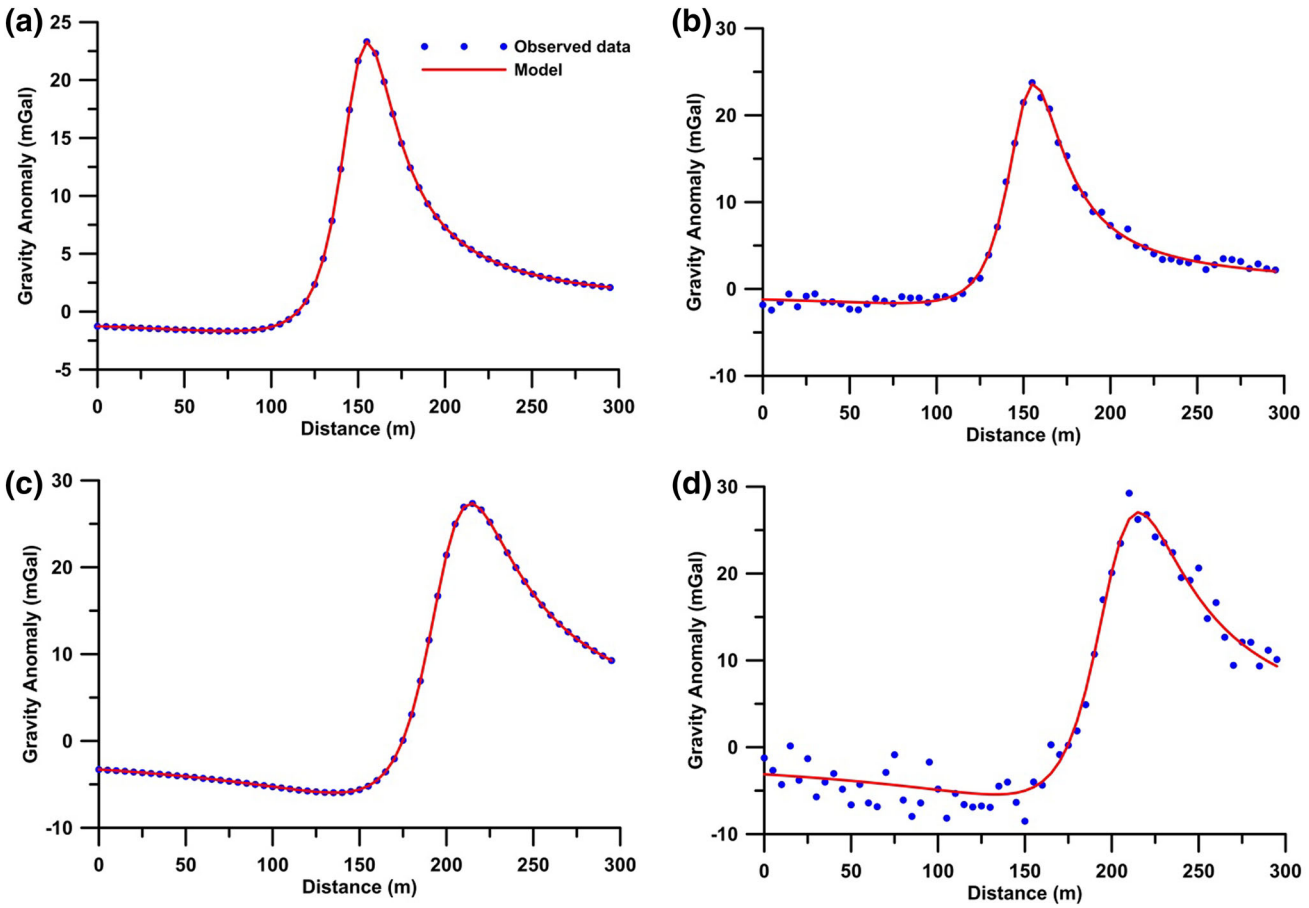

Fig. 5 Gravity data: fittings between the observed and model data for Thin sheet: Model 1- **a** noise-free synthetic data and **b** 10 % Gaussian noisy synthetic data, and Model 2- **c** noise-free synthetic data and **d** 20 % Gaussian noisy synthetic data

Table 2 Actual model parameters, search range and interpreted mean model for noise free and 20 % Gaussian noise with uncertainty-Gravity data (Model 2)

Model parameters	Actual value	Search range	Mean model	
			Noise-free	Noisy
k (mGal)	1000	0–2000	1000.3 ± 2.5	1006.2 ± 4.3
x_0 (m)	200	0–500	200.0 ± 0.0	201.7 ± 0.2
z (m)	30	0–50	30.0 ± 0.0	30.8 ± 0.2
θ (°)	40	0–90	40.0 ± 0.0	41.7 ± 0.2
Misfit			8.1×10^{-10}	5.1×10^{-3}

$$\varphi = \frac{1}{\mathrm{N}} \sum_{i=1}^{\mathrm{N}} \left(\frac{V_i^0 - V_i^c}{|V_i^0| + (V_{max}^0 - V_{min}^0)/2} \right)^2 \quad (3)$$

where N is number of data point, V_i^0 and V_i^c are the *ith* observed and model responses and $V_{\max}^0$ and $V_{\min}^0$ are the maximum and minimum values of the observed response, respectively.

The detailed VFSA algorithm is not discussed here and referred the work of Sen and Stoffa (2013), Sharma (2012) and Sharma and Biswas (2013), Biswas (2015). In VFSA optimization, parameters such as Initial temperature 1.0, cooling schedule 0.4, number of iterations 2000 and number of moves per temperature 50 is used in the present study. Global model, Probability Density Function (PDF) and Uncertainty analysis has been done based on the techniques developed by Mosegaard and Tarantola (1995) and Sen and Stoffa (1996).

The code was developed in Window 7 environment using MS FORTRAN Developer studio on a simple desktop PC with Intel Pentium Processor. For each step of optimization, a total of 10^6 forward computations (2000 iteration × 50 number of moves × 10 VFSA runs) were performed and accepted models stored in memory.

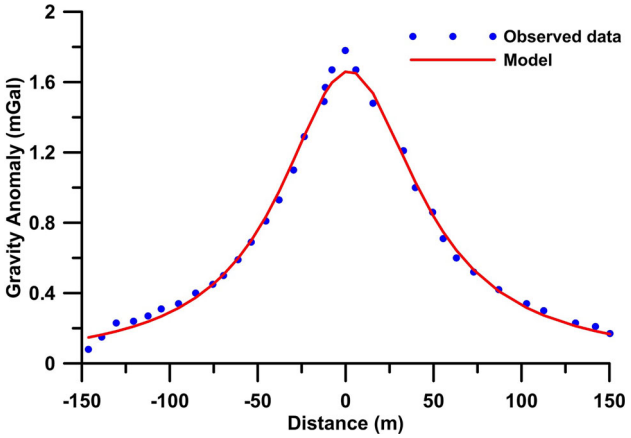

Fig. 6 Fittings between the observed and model data for Mobrun Anomaly, Noranda, Quebec, Canada

Results and discussion

Gravity data

Synthetic example

The VFSA global optimization is instigated using noise-free and noisy synthetic data (10 and 20 % Gaussian noise) for gravity anomaly over a thin sheet type model. Initially, all model parameters are optimized for each data set.

Model 1 Firstly, synthetic data are generated using Eq. (1) for a sheet model (Table 1) and 10 % Gaussian noise is added to the synthetic data. Inversion is implemented using noise-free and noisy synthetic data to retrieve the actual model parameters and study the effect of noise on the interpreted model parameters. Primarily, a suitable search range for each model parameter is selected and a single VFSA optimization is executed. After studying the proper convergence of each model parameter (k, x_0, z, and θ) and misfit (Fig. 2) by adjusting VFSA parameters (such as initial temperature, cooling schedule, number of moved per temperature and number of iterations), 10 VFSA runs are performed. Then, histograms (Fig. 3a) are prepared using accepted models whose misfit is lower than 10^{-4}. The histograms in Fig. 3a depict that all model parameters (k, x_0, z, and θ) show closer to the actual solution. A statistical mean model is also computed using models that have misfit lower than 10^{-4} and lie within one standard deviation. Table 1 depicts that the estimated mean model and uncertainty.

Figure 4a depicts cross-plots for noise free data between the model parameters k, z, and θ using accepted models with misfit lower than 10^{-4} (green) and models within the pre-defined high PDF region (red). This shows that all parameters are well resolved and pointing towards its actual value and there is no uncertainty in each model parameters. Figure 5a depicts a comparison between the observed and the mean model response.

Next, VFSA optimization is performed using 10 % Gaussian noise added data for Model 1 (Table 1). The convergence of each model parameter and reduction of misfit is studied for a single solution. After observing the reduction of misfit systematically and stabilization of each model parameter during later iteration, ten VFSA runs are performed. The histograms in Fig. 3b also depict that all model parameters (k, x_0, z, and θ) show closer to the actual solution. A statistical mean model is also computed using models that have misfit lower than 10^{-2} and lie within one standard deviation. Table 1 depicts that the estimated mean model and uncertainty for noisy model.

Figure 4b depicts cross-plots for noisy data between the model parameters k, z, and θ using accepted models with

Table 3 Search range and interpreted mean model for Mobrun Anomaly, Noranda, Quebec, Canada

Model parameters	Search range	Mean model (VFSA)	Biswas 2015
k (mGal)	0–100	79.5 ± 0.5	79.5 ± 0.7
x_0 (m)	−5 to 5	1.4 ± 0.4	2.5 ± 0.4
z (m)	0–60	47.9 ± 0.4	47.7 ± 0.6
θ (°)	0–180	88.7 ± 0.4	–
Misfit		6.2×10^{-4}	6.5×10^{-4}

Table 4 Actual model parameters, search range and interpreted mean model for noise free and 10 % Gaussian noise with uncertainty-Magnetic data (**Model 1**)

Model parameters	Actual value	Search range	Mean model (noise-free) (noisy)	
k (nT)	200	0–500	200.0 ± 0.3	199.7 ± 1.0
x_0 (m)	150	0–300	150.0 ± 0.0	150.0 ± 0.1
z (m)	10	0–20	10.0 ± 0.0	9.8 ± 0.1
θ (°)	45	0–90	45.0 ± 0.0	45.5 ± 0.3
Misfit			6.3×10^{-9}	5.9×10^{-4}

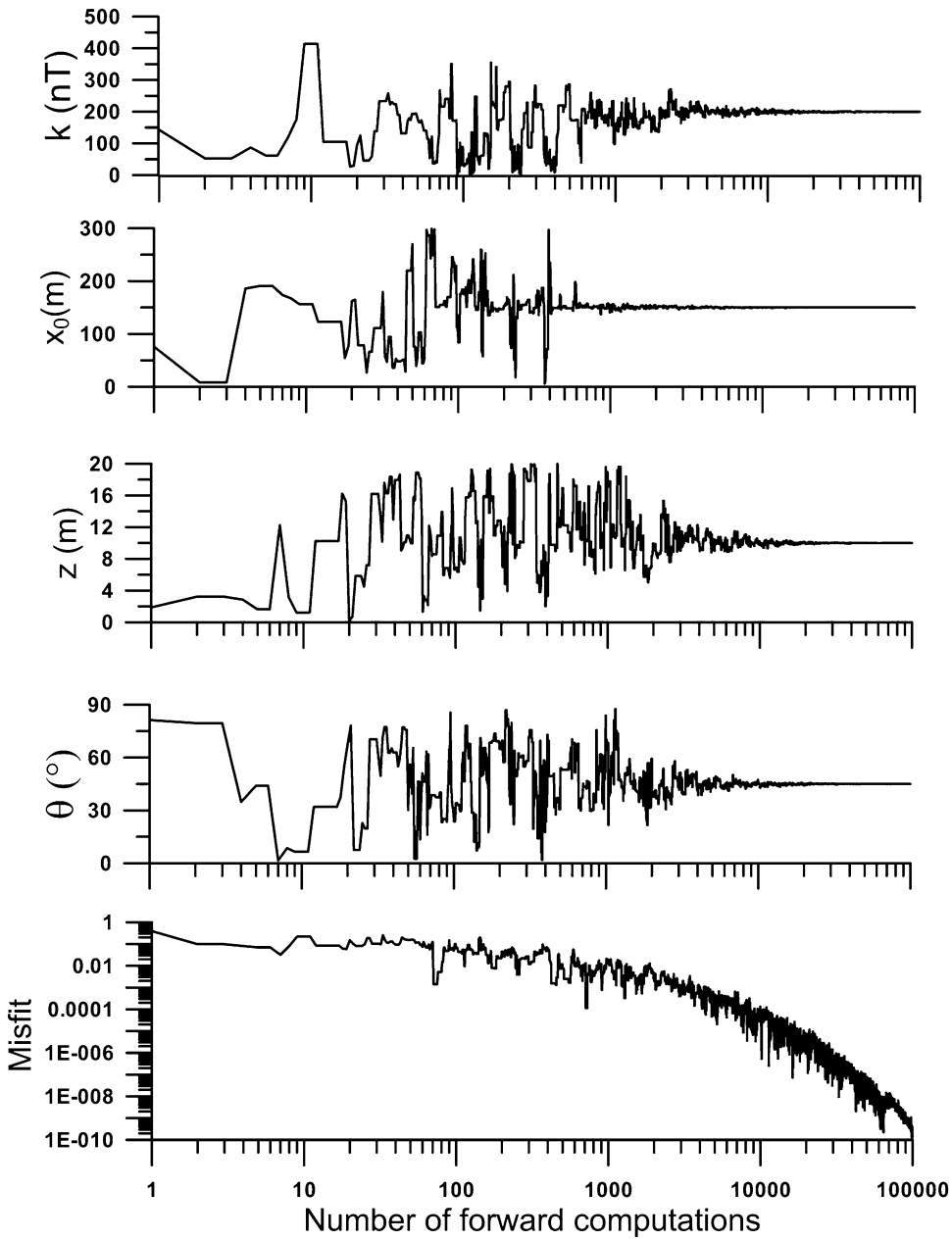

Fig. 7 Convergence Pattern for various model parameters and misfit for magnetic data

misfit lower than 10^{-4} (green) and models within the pre-defined high PDF region (red). However, it reveals that scatter is large for noisy data but models in high PDF region are restricted near the actual value. Figure 5b depicts a comparison between the observed and the mean model response for noisy data.

Model 2 Another synthetic data are generated using Eq. (1) for a sheet model (Table 2) and 20 % Gaussian noise is added to the synthetic data to check the effect of more noise. Inversion is implemented using noise-free and noisy synthetic data to retrieve the actual model parameters and study the effect of higher noise on the interpreted model parameters. The procedure was repeated again as discussed in Model 1. The histogram and cross plots were also studied and found the similar in nature like Model 1. For brevity, the figures are not presented here. Figure 5c, d depicts a comparison between the observed and the mean model response for noise free and noisy data.

Field example

Mobrun Anomaly, Noranda, Quebec, Canada Residual gravity anomaly map over Noranda Mining District, Quebec, Canada was taken (Grant and West 1965; Roy et al. 2000) over a massive sulphide ore body (Fig. 6). The

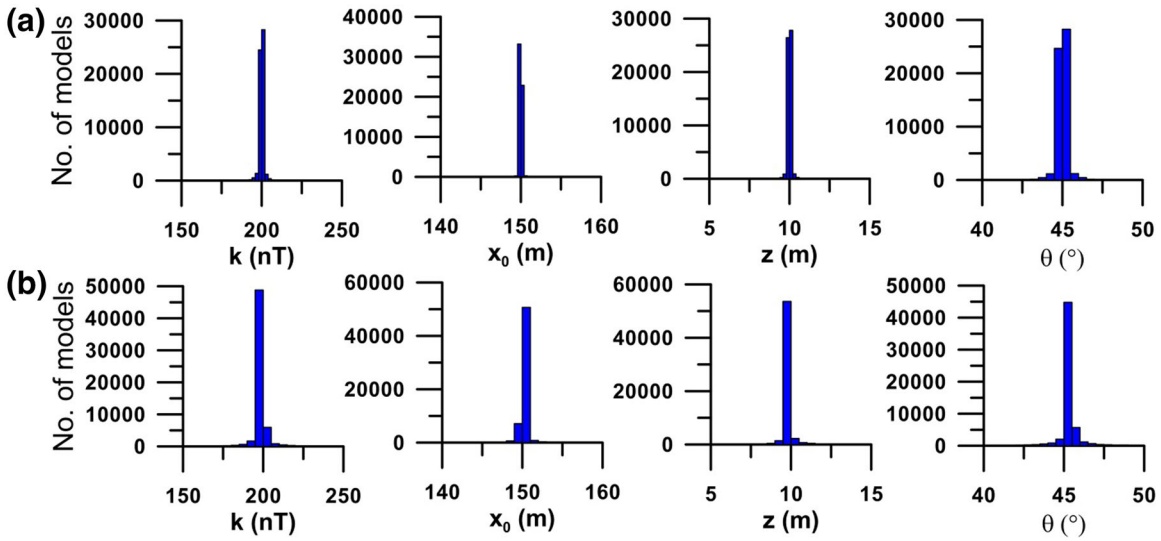

Fig. 8 Magnetic data: **a** histograms of all accepted models having misfit $<10^{-4}$ for noise-free synthetic data for thin sheet-Model 1 and **b** histograms of all accepted models having misfit $<10^{-2}$ for noisy synthetic data for Thin sheet-Model 2

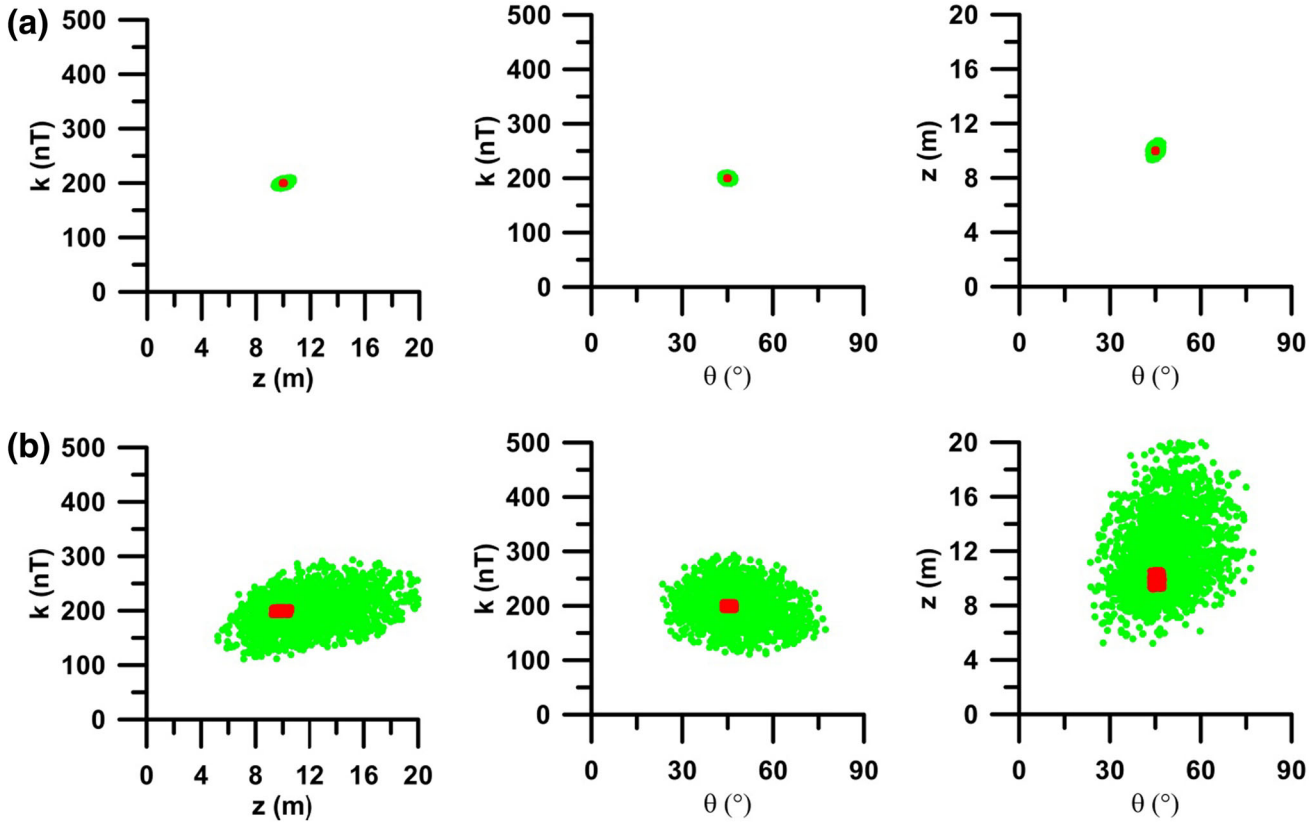

Fig. 9 Magnetic data: **a** *scatter-plots* between amplitude coefficient (k), depth (z), magnetization angle (θ) for all models having misfit <threshold (10^{-4} for noise-free data) (*green*), and models with PDF >60.65 % (*red*) for noise free data; **b** *scatter-plots* between amplitude coefficient (k), depth (z), magnetization angle (θ) for all models having misfit <threshold (10^{-2} for noisy data) (*green*), and models with PDF >60.65 % (*red*) for noisy data

interpretation procedure mentioned in synthetic example is again carried out for this field data. The interpreted results are shown in Table 3. Figure 6 depicts the fitting between the observed and interpreted mean model response. The depth of the body estimated in the present study is 47.9 m and is in excellent agreement with the depth obtained by

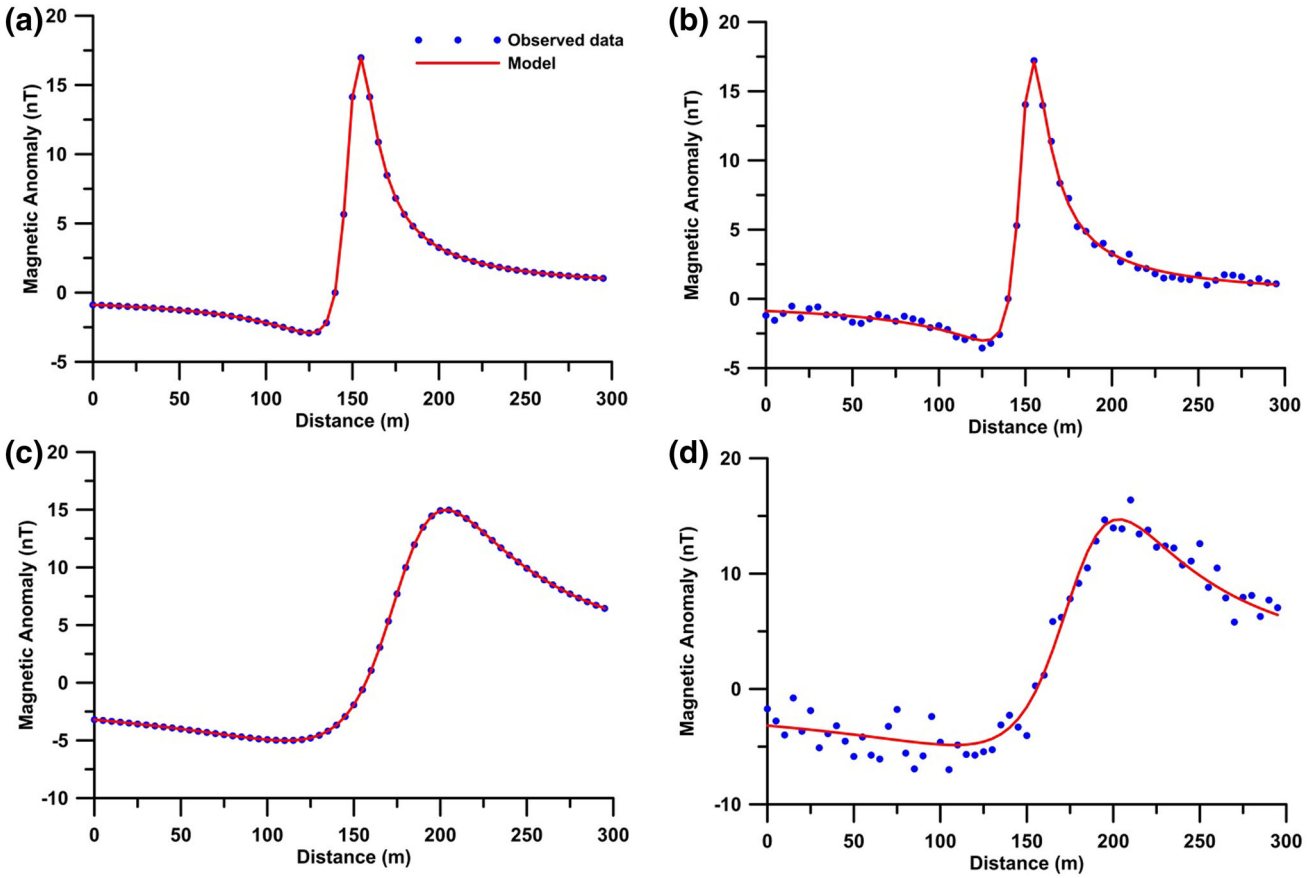

Fig. 10 Magnetic data: fittings between the observed and model data for Thin sheet: Model 1- **a** noise-free synthetic data and **b** 10 % Gaussian noisy synthetic data, and Model 2- **c** noise-free synthetic data and **d** 20 % Gaussian noisy synthetic data

Table 5 Actual model parameters, search range and interpreted mean model for noise free and 20 % Gaussian noise with uncertainty magnetic data (Model 2)

Model parameters	Actual value	Search range	Mean model	
			Noise-free	Noisy
k (nT)	800	0–1000	801.7 ± 2.1	807.2 ± 3.2
x_0 (m)	180	0–300	180.0 ± 0.0	179.6 ± 0.2
z (m)	40	0–50	40.0 ± 0.0	40.9 ± 0.2
θ (°)	60	0–90	60.0 ± 0.0	59.8 ± 0.2
Misfit			5.3×10^{-8}	5.9×10^{-3}

Biswas 2015. Also, the misfit in the present approach is slightly less than the other method. However, it should be mentioned that Biswas 2015 interpreted this field data using horizontal cylinder, however, in the present case, it is interpreted as thin sheet type structure.

Magnetic data

Synthetic example

The VFSA global optimization is also applied using noise-free and noisy synthetic data (10 and 20 % Gaussian noise) for magnetic anomaly over a thin sheet type model. Initially, all model parameters are optimized for each data set.

Model 1 Firstly, synthetic data are generated using Eq. (2) for a sheet model (Table 4) and 10 % Gaussian noise is added to the synthetic data. Like in gravity data, inversion is implemented using noise-free and noisy synthetic data to retrieve the actual model parameters and study the effect of noise on the interpreted model parameters. Figure 7 shows the convergence pattern for all model parameters. The inversion procedure mentioned for gravity data is also applied here and is not repeated here for

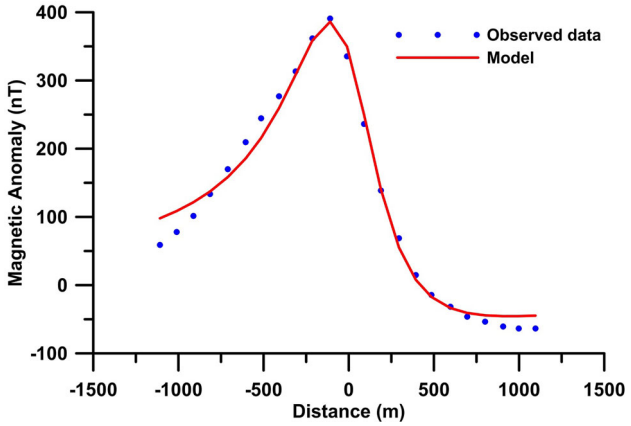

Fig. 11 Fittings between the observed and model data for Pishabo Lake anomaly, Canada

Table 6 Search range and interpreted mean model for Pishabo Lake anomaly, Canada

Model parameters	Search range	Mean model (VFSA)
k (nT)	0–1000000	141187.3 ± 610.5
x_0 (m)	−50 to 50	1.7 ± 1.4
z (m)	10–500	324.0 ± 1.4
θ (°)	−90 to 90	−37.9 ± 0.2
Misfit		2.5×10^{-3}

brevity. Figure 8a shows the histogram for all model parameters (k, x_0, z, and θ) is closer to the actual solution. A statistical mean model is also computed for magnetic anomaly using models that have misfit lower than 10^{-4} and lie within one standard deviation. Table 4 depicts that the estimated mean model and uncertainty.

Figure 9a depicts cross-plots for noise free data between the model parameters k, z, and θ using accepted models with misfit lower than 10^{-4} (green) and models within the pre-defined high PDF region (red). This also shows that all parameters are well resolved and pointing towards its actual value and there is no uncertainty in each model parameters. Figure 10a depicts a comparison between the observed and the mean model response.

VFSA optimization is performed using 10 % Gaussian noise added data for Model 1 (Table 4). The histograms in Fig. 8b also depict that all model parameters (k, x_0, z, and θ) show closer to the actual solution. A statistical mean model is also computed using models that have misfit lower than 10^{-4} and lie within one standard deviation. Table 4 depicts that the estimated mean model and uncertainty for noisy model.

Figure 4b depicts cross-plots for noisy data between the model parameters k, z, and θ using accepted models with misfit lower than 10^{-4} (green) and models within the pre-defined high PDF region (red). As, it is a noisy data the scatter is large but models in high PDF region are restricted near the actual value. Figure 10b depicts a comparison between the observed and the mean model response for noisy data.

Model 2 Alternative synthetic data are also generated using Eq. (2) for a sheet model (Table 5) and 20 % Gaussian noise is added to the synthetic data to check the effect of more noise. Inversion is executed using noise-free and noisy synthetic data to retrieve the actual model parameters and study the effect of higher noise on the interpreted model parameters. The procedure was repeated again as discussed in Model 1 for magnetic data. The histogram and cross plots were also studied and found the similar in nature like Model 1. For brevity, the figures are not presented here. Figure 10c, d depicts a comparison between the observed and the mean model response for noise free and noisy data.

Field example

Pishabo Lake anomaly, Canada

Total magnetic anomaly from Pishabo Lake, Ontario (McGrath 1970) was taken from an olivine diabase dike (Fig. 11). The interpretation process mentioned in synthetic example is again applied for this field data. The interpreted results are shown in Table 6. Figure 11 depicts the fitting between the observed and interpreted mean model response. The depth of the body estimated in the present study is 324 m and is in excellent agreement with the depth obtained by Abdelrahman et al. (2012). Moreover, the depth and shape of the concealed structure obtained by the present method approve very sound with the surface geologic records shown by McGrath (1970).

Conclusions

A proficient and reliable method is employed for the interpretation of gravity and magnetic anomaly over thin sheet type structure using a VFSA global optimization method for exploration studies. The problematic determination of the appropriate shape, depth, index parameter and amplitude coefficient of a buried structure from a residual gravity and magnetic anomaly profile can be well resolved using the present method. The present study discloses that, while optimizing all model parameters (amplitude coefficient, location, depth, angle) together, the VFSA approach yields a very good results without any uncertainty in the final model parameters. The efficacy of this approach has been successfully proved, established and validated using noise-free and noisy synthetic data. The metier of this

method for practical application in mineral exploration has also been efficaciously exemplified on some field examples with many complex geological structures and depths of burial. The estimated gravity and magnetic inverse parameters for the field data are found to be in excellent agreement with the other methods as well as from the geological and drilling results. The actual (not CPU) time for the whole computation process is nearly 35 s.

References

Abdelrahman EM (1990) Discussion on ''a least-squares approach to depth determination from gravity data'' by GUPTA, O.P. Geophysics 55:376–378

Abdelrahman EM (1994) A rapid approach to depth determination from magnetic anomalies due to simple geometrical bodies. J Univ Kuwait Sci 21:109–115

Abdelrahman EM, El-Araby TM (1993) A least-squares minimization approach to depth determination from moving average residual gravity anomalies. Geophysics 59:1779–1784

Abdelrahman EM, Essa KS (2015) A new method for depth and shape determinations from magnetic data. Pure Appl Geophys 172(2):439–460

Abdelrahman EM, Sharafeldin SM (1995a) A least-squares minimization approach to depth determination from numerical horizontal gravity gradients. Geophysics 60:1259–1260

Abdelrahman EM, Sharafeldin SM (1995b) A least-squares minimization approach to shape determination from gravity data. Geophysics 60:589–590

Abdelrahman EM, Sharafeldin SM (1996) An iterative least-squares approach to depth determination from residual magnetic anomalies due to thin dikes. Appl Geophys 34:213–220

Abdelrahman EM, Bayoumi AI, Abdelhady YE, Gobash MM, EL-Araby HM (1989) Gravity interpretation using correlation factors between successive least—squares residual anomalies. Geophysics 54:1614–1621

Abdelrahman EM, Bayoumi AI, El-Araby HM (1991) A least-squares minimization approach to invert gravity data. Geophysics 56:115–118

Abdelrahman EM, El-Araby TM, El-Araby HM, Abo-Ezz ER (2001a) Three least squares minimization approaches to depth, shape, and amplitude coefficient determination from gravity data. Geophysics 66:1105–1109

Abdelrahman EM, El-Araby TM, El-Araby HM, Abo-Ezz ER (2001b) A New method for shape and depth determinations from gravity data. Geophysics 66:1774–1780

Abdelrahman EM, Abo-Ezz ER, Essa KS (2012) Parametric inversion of residual magnetic anomalies due to simple geometric bodies. Explor Geophys 43:178–189

Asfahani J, Tlas M (2004) Nonlinearly constrained optimization theory to interpret magnetic anomalies due to vertical faults and thin dikes. Pure Appl Geophys 161:203–219

Asfahani J, Tlas M (2007) A robust nonlinear inversion for the interpretation of magnetic anomalies caused by faults, thin dikes and spheres like structure using stochastic algorithms. Pure Appl Geophys 164:2023–2042

Asfahani J, Tlas M (2012) Fair function minimization for direct interpretation of residual gravity anomaly profiles due to spheres and cylinders. Pure Appl Geophys 169:157–165

Bhattacharyya BK (1965) Two-dimensional harmonic analysis as a tool for magnetic interpretation. Geophysics 30:829–857

Biswas A (2015) Interpretation of residual gravity anomaly caused by a simple shaped body using very fast simulated annealing global optimization. Geosci Front 6(6):875–893

Biswas A, Sharma SP (2014a) Resolution of multiple sheet-type structures in self-potential measurement. J Earth Syst Sci 123(4):809–825

Biswas A, Sharma SP (2014b) Optimization of self-potential interpretation of 2-D inclined sheet-type structures based on very fast simulated annealing and analysis of ambiguity. J Appl Geophys 105:235–247

Biswas A, Sharma SP (2015) Interpretation of self-potential anomaly over idealized body and analysis of ambiguity using very fast simulated annealing global optimization. Near Surf Geophys 13(2):179–195

Biswas A, Sharma SP (2016) Integrated geophysical studies to elicit the structure associated with Uranium mineralization around South Purulia Shear Zone, India: a review. Ore Geol Rev 72:1307–1326

Biswas A, Mandal A, Sharma SP, Mohanty WK (2014a) Delineation of subsurface structure using self-potential, gravity and resistivity surveys from South Purulia Shear Zone, India: implication to uranium mineralization. Interpretation 2(2):T103–T110

Biswas A, Mandal A, Sharma SP, Mohanty WK (2014b) Integrating apparent conductance in resistivity sounding to constrain 2D gravity modeling for subsurface structure associated with Uranium mineralization across South Purulia Shear Zone, West Bengal, India. Int J Geophys 2014:1–8, Article ID 691521. doi:10.1155/2014/691521

Bowin C, Scheer E, Smith W (1986) Depth estimates from ratios of gravity, geoid and gravity gradient anomalies. Geophysics 51:123–136

Dosso SE, Oldenburg DW (1991) Magnetotelluric appraisal using simulated annealing. Geophys J Int 106:370–385

Elawadi E, Salem A, Ushijima K (2001) Detection of cavities from gravity data using a neural network. Explor Geophys 32:75–79

Essa KS (2012) A fast interpretation method for inverse modelling of residual gravity anomalies caused by simple geometry. J Geol Res 2012:1–10, Article ID 327037. doi:10.1155/2012/327037

Essa KS (2013) New fast least-squares algorithm for estimating the best-fitting parameters due to simple geometric-structures from gravity anomalies. J Adv Res 5(1):57–65

Fedi M (2007) DEXP: a fast method to determine the depth and the structural index of potential fields sources. Geophysics 72(1):I1–I11

Gay SP (1963) Standard curves for the interpretation of magnetic anomalies over long tabular bodies. Geophysics 28:161–200

Gay SP (1965) Standard curves for the interpretation of magnetic anomalies over long horizontal cylinders. Geophysics 30:818–828

Gokturkler G, Balkaya C (2012) Inversion of self-potential anomalies caused by simple geometry bodies using global optimization algorithms. J Geophys Eng 9:498–507

Grant RS, West GF (1965) Interpretation theory in applied geophysics. McGraw-Hill Book Co, New York

Gupta OP (1983) A Least-squares approach to depth determination from gravity data. Geophysics 48:360–375

Hartmann RR, Teskey D, Friedberg I (1971) A system for rapid digital aeromagnetic interpretation. Geophysics 36:891–918

Jain S (1976) An automatic method of direct interpretation of magnetic profiles. Geophysics 41:531–541

Juan LFM, Esperanza G, José GPFÁ, Heidi AK, César OMP (2010) PSO: a powerful algorithm to solve geophysical inverse problems: application to a 1D-DC resistivity case. J Appl Geophys 71:13–25

Kilty TK (1983) Werner deconvolution of profile potential field data. Geophysics 48:234–237

Lines LR, Treitel S (1984) A review of least-squares inversion and its application to geophysical problems. Geophys Prospect 32:159–186

Mandal A, Biswas A, Mittal S, Mohanty WK, Sharma SP, Sengupta D, Sen J, Bhatt AK (2013) Geophysical anomalies associated with uranium mineralization from Beldih mine, South Purulia Shear Zone, India. J Geol Soc India 82(6):601–606

Mandal A, Mohanty WK, Sharma SP, Biswas A, Sen J, Bhatt AK (2015) Geophysical signatures of uranium mineralization and its subsurface validation at Beldih, Purulia District, West Bengal, India: a case study. Geophys Prospect 63:713–724

McGrath H (1970) The dipping dike case: a computer curve-matching method of magnetic interpretation. Geophysics 35(5):831

McGrath PH, Hood PJ (1973) An automatic least-squares multimodel method for magnetic interpretation. Geophysics 38(2):349–358

Mehanee S (2014) Accurate and efficient regularized inversion approach for the interpretation of isolated gravity anomalies. Pure Appl Geophys 171(8):1897–1937

Mohan NL, Sundararajan N, Seshagiri Rao SV (1982) Interpretation of some two-dimensional magnetic bodies using Hilbert transforms. Geophysics 46:376–387

Mohan NL, Anandababu L, Roa S (1986) Gravity interpretation using Mellin transform. Geophysics 52:114-122

Mosegaard K, Tarantola A (1995) Monte Carlo sampling of solutions to inverse problems. J Geophys Res 100(B7):12431–12447

Nettleton LL (1962) Gravity and magnetics for geologists and seismologists. AAPG 46:1815–1838

Nettleton, L. L., (1976) Gravity and Magnetics in Oil Prospecting. McGraw-Hill Book Co, 1976

Odegard ME, Berg JW (1965) Gravity interpretation using the fourier integral. Geophysics 30:424–438

Prakasa Rao TKS, Subrahmanyan M, Srikrishna Murthy A (1986) Nomograms for direct interpretation of magnetic anomalies due to long horizontal cylinders. Geophysics 51:2150–2159

Rothman DH (1985) Nonlinear inversion, statistical mechanics and residual statics estimation. Geophysics 50:2784–2796

Rothman DH (1986) Automatic estimation of large residual statics correction. Geophysics 51:337–346

Roy L, Agarwal BNP, Shaw RK (2000) A new concept in Euler deconvolution of isolated gravity anomalies. Geophys Prospect 48:559–575

Salem A, Ravat D (2003) A combined analytic signal and Euler method (AN-EUL) for automatic interpretation of magnetic data. Geophysics 68(6):1952–1961

Sen MK, Stoffa PL (1996) Bayesian inference, Gibbs sampler and uncertainty estimation in geophysical inversion. Geophys Prospect 44:313–350

Sen MK, Stoffa PL (2013) Global optimization methods in geophysical inversion, 2nd edn. Cambridge Publisher, London

Sharma SP (2012) VFSARES—a very fast simulated annealing FORTRAN program for interpretation of 1-D DC resistivity sounding data from various electrode array. Comput Geosci 42:177–188

Sharma SP, Biswas A (2011) Global nonlinear optimization for the estimation of static shift and interpretation of 1-D magnetotelluric sounding data. Ann Geophys 54(3):249–264

Sharma SP, Biswas A (2013) Interpretation of self-potential anomaly over a 2D inclined structure using very fast simulated-annealing global optimization—an insight about ambiguity. Geophysics 78:WB3–WB15

Sharma B, Geldart LP (1968) Analysis of gravity anomalies of two-dimensional faults using Fourier transforms. Geophys Prospect 16:77–93

Sharma SP, Kaikkonen P (1998) Two-dimensional nonlinear inversion of VLF-R data using simulated annealing. Geophys J Int 133:649–668

Sharma SP, Kaikkonen P (1999a) Appraisal of equivalence and suppression problems in 1-D EM and DC measurements using global optimization and joint inversion. Geophys Prospect 47:219–249

Sharma SP, Kaikkonen P (1999b) Global optimisation of time domain electromagnetic data using very fast simulated annealing. Pure Appl Geophys 155:149–168

Shaw RK, Agarwal BNP (1990) The application of Walsh transforms to interpret gravity anomalies due to some simple geometrically shaped causative sources: a feasibility study. Geophysics 55:843–850

Silva JBC (1989) Transformation of nonlinear problems into linear ones applied to the magnetic field of a two-dimensional prism. Geophysics 54:114–121

Singh A, Biswas A (2016) Application of global particle swarm optimization for inversion of residual gravity anomalies over geological bodies with idealized geometries. Nat Resour Res. doi:10.1007/s11053-015-9285-9

Siva Kumar Sinha GDJ, Ram Babu HV (1985) Analysis of gravity gradient over a thin infinite sheet. Proc Indian Acad Sci Earth Planet Sci 94(1):71–76

Thompson DT (1982) EULDPH-a new technique for making computer-assisted depth estimates from magnetic data. Geophysics 47:31–37

Tlas M, Asfahani J (2011a) Fair function minimization for interpretation of magnetic anomalies due to thin dikes, spheres and faults. J Appl Geophys 75:237–243

Tlas M, Asfahani J (2011b) A new-best-estimate methodology for determining magnetic parameters related to field anomalies produced by buried thin dikes and horizontal cylinder-like structures. Pure Appl Geophys 168:861–870

Tlas M, Asfahani J (2015) The simplex algorithm for best-estimate of magnetic parameters related to simple geometric-shaped structures. Math Geosci 47(3):301–316

Tlas M, Asfahani J, Karmeh H (2005) A versatile nonlinear inversion to interpret gravity anomaly caused by a simple geometrical structure. Pure Appl Geophys 162:2557–2571

Zhao LS, Sen MK, Stoffa PL, Frohlich C (1996) Application of very fast simulated annealing to the determination of the crustal structure beneath tibet. Geophys Prospect 125:355–370